





Cite this: *J. Mater. Chem. C*, 2022,  
10, 15883

# Optimizing chain alignment and preserving the pristine structure of single-ether based PBTTT helps improve thermoelectric properties in sequentially doped thin films†

Huiyan Zeng,<sup>a</sup> Pablo Durand,<sup>b</sup> Shubhradip Guchait,<sup>a</sup> Laurent Herrmann,<sup>a</sup>  
Céline Kiefer,<sup>c</sup> Nicolas Leclerc <sup>\*b</sup> and Martin Brinkmann <sup>\*a</sup>

Doped polymer semiconductors are of central interest in material science for their interesting charge transport and thermoelectric properties. Polymer alignment and crystallization are two means to enhance thermoelectric parameters (charge conductivity  $\sigma$  and Seebeck coefficient  $S$ ) in the polymer chain direction. In this study, we focus on the thermoelectric properties of a PBTTT polymer semiconductor bearing linear heptyl-oxy-butyl ( $C_7OC_4$ ) side chains (PBTTT- $^8O$ ) in thin oriented films aligned by high-temperature rubbing. Both the degree of in-plane orientation and the preferential contact plane of the polymer are determined by the rubbing temperature that can be tuned in a large 25–240 °C range. Optimal TE properties with high charge conductivities in the  $2\text{--}5 \times 10^4 \text{ S cm}^{-1}$  range and power factors  $>2.0 \text{ mW m}^{-1} \text{ K}^{-2}$  are obtained in the chain direction only when the film orientation is optimized (dichroic ratio  $>20$ ). Contrary to other dopants such as  $FeCl_3$ , the structure of PBTTT- $^8O$  is little modified by the inclusion of  $F_6TCNNQ$  dopant molecules in the layers of disordered side chains. UV-vis-NIR spectroscopy shows that dimer formation of the radical anion  $F_6TCNNQ^{\bullet-}$  explains this behavior. Overall, this study demonstrates that the highest thermoelectric performances for a given polymer/dopant system can only be uncovered when the optimal conditions for polymer semiconductor growth/alignment and sequential doping are found. In addition, the  $S\text{--}\sigma$  scaling laws along and perpendicular to the chain direction are (i) independent of the chemical nature of side chains and dopants and (ii) essentially determined by the level of chain alignment and molecular packing of PBTTT backbones.

Received 26th August 2022,  
Accepted 28th September 2022

DOI: 10.1039/d2tc03600b

rsc.li/materials-c

## 1. Introduction

Polymer semiconductors (PSCs) are highly versatile materials widely used for the design of numerous electronic devices such as Organic Field Effect Transistors (OFETs), Organic Light Emitting Diodes (OLEDs) and organic solar cells.<sup>1</sup> More recently, remarkable thermoelectric properties were evidenced for conducting polymers, doped PSCs and hybrid materials.<sup>2–5</sup> Thermoelectric materials are of interest as they have the ability to convert a temperature gradient into an electric voltage thanks to the Seebeck effect. To be effective, a thermoelectric material must have a high charge conductivity  $\sigma$  and a high

Seebeck coefficient  $S$  as well as a moderate thermal conductivity  $\kappa$ . Polymeric TE materials have multiple advantages related to their flexibility, ease of processing and versatility thanks to the large palette of molecular structures accessible *via* adequate chemical engineering.<sup>4,5</sup> Intrinsically, PSCs show a low thermal conductivity that is only moderately increased upon doping and/or alignment.<sup>6</sup> In order to become conductive and efficient for TE applications, polymer semiconductors must be doped in a controlled manner.<sup>7</sup> This is why doping PSCs is a central step in the fabrication of TE materials in order to tune the charge density and hence, charge conductivity and Seebeck coefficient. The precise localization of dopants in the polymer is pivotal since it determines the magnitude of Coulombic interactions between the charge carriers on the polymer backbones (polarons and bipolarons) and the ionized dopant molecules hosted in the PSC crystals as well as the polymer packing order.<sup>8–10</sup> From that perspective, sequential doping of PSCs proved to be a very effective processing strategy towards conducting polymers of high conductivity since it allows a high crystallinity of the pristine

<sup>a</sup> Université de Strasbourg, CNRS, ICS UPR 22, F-67000 Strasbourg, France.  
E-mail: martin.brinkmann@ics-cnrs.unistra.fr

<sup>b</sup> Université de Strasbourg, CNRS, ICPEES UMR 7515, F-67087 Strasbourg, France.  
E-mail: leclercn@unistra.fr

<sup>c</sup> Université de Strasbourg, CNRS, IPCMS UMR 7504, F-67087 Strasbourg, France

† Electronic supplementary information (ESI) available. See DOI: <https://doi.org/10.1039/d2tc03600b>



polymer films to be preserved.<sup>11–16</sup> It has also been shown that introduction of short ethylene glycol side chains can be an effective means to enhance the TE properties of the PSC without modifying the packing of its backbone.<sup>17</sup> Recently, it was reported that the use of PSCs bearing alkyl side chains comprising a single ether group helped reach very high conductivities of up to  $5 \times 10^4 \text{ S cm}^{-1}$  and TE power factors of  $2.9 \text{ mW m}^{-1} \text{ K}^{-2}$  in aligned thin films.<sup>18</sup>

Control of chain orientation and crystallinity allows further enhancement of TE properties as both thermopower  $S$  and charge conductivity  $\sigma$  can be enhanced in the direction of chain alignment.<sup>19–26</sup> Dopant intercalation in the host polymer impacts the structure of the doped polymer and can induce disorder that is detrimental in some cases for charge transport properties. The dopant position and the way it is intercalated in the crystals of the polymer semiconductors depend on the dopant dimensions and the length of alkyl side chains.<sup>20–24</sup> Yet, no work has focused on the role of the dominant contact plane of the crystals on TE performances. For most PSCs, the processing conditions (temperature, solvent, film preparation method) determine the dominant contact planes of the crystals on a substrate.<sup>26–30</sup> For P3HT and PBTTT, different crystal orientations on a substrate are observed depending on the type of solvent used, the temperature of an annealing step or the molecular weight of the polymer. In this work, we have studied the way the growth conditions (rubbing temperature  $T_R$ ) of oriented PSC thin films affect the resulting anisotropic TE properties in the doped thin films. Indeed, for polymer semiconductors such as P3HT or PBTTT, it has been shown that the temperature at which a thin film is oriented by rubbing impacts its orientation and structure.<sup>31,32</sup> In particular, for P3HT, the size of crystalline lamellae and the total crystallinity are controlled by  $T_R$  and determine the obtained TE properties in films doped with  $F_4\text{TCNQ}$ .

In this study, we focus on the previously published PBTTT-<sup>8</sup>O bearing  $n\text{-C}_7\text{-O-C}_4$  side chains and we used 1,3,4,5,7,8-hexafluoro-tetracyanonaphtho-quinodimethane ( $F_6\text{TCNNQ}$ ) as the dopant.<sup>16</sup> Interestingly, the use of single-ether side chains makes it possible to align the PBTTT polymer in a large temperature range (100–240 °C), and thus to prepare aligned films with different contact planes of the crystals on the substrate. Sequential doping with  $F_6\text{TCNNQ}$  was used and in particular the increasing concentration doping (ICD) method was implemented. In this method, for a given final doping level, the sample is progressively doped at multiple and increasing concentrations of dopants in an orthogonal solvent (acetonitrile).<sup>33</sup> In this way, the dopant molecules are introduced progressively in the crystal lattice of the polymer, reducing structural damages by fast and uncontrolled intercalation. When oriented at 170 °C, thin films of PBTTT-<sup>8</sup>O, doped by ICD, can show remarkable TE properties with charge conductivities that can reach  $2\text{--}5 \times 10^4 \text{ S cm}^{-1}$  and TE PF of  $2.9 \text{ mW m}^{-1} \text{ K}^{-2}$ . The enhanced TE performances have been attributed to (i) the higher in-plane orientation achieved over PBTTT with linear side chains such as PBTTT- $\text{C}_{12}$  and (ii) to the random orientation of intercalated  $F_6\text{TCNNQ}$  dopants in the disordered layers of  $n\text{-C}_7\text{-O-C}_4$  side

chains that help screen more effectively the polaron-anion Coulombic interactions and help thus achieve larger charge carrier mobilities.

In this contribution, we propose to follow the influence of the alignment conditions on the TE properties in PBTTT-<sup>8</sup>O films doped with  $F_6\text{TCNNQ}$ .  $F_6\text{TCNNQ}$  has been chosen as it is as rather stable conjugated dopant with an electron affinity  $E_A = 5.37 \text{ eV}$  that can readily oxidize PBTTT-<sup>8</sup>O and leads to rather high stability of the doped system under inert atmosphere.<sup>34</sup> In particular, we focus on the impact of the rubbing temperature  $T_R$  on the orientation and contact plane of the PBTTT-<sup>8</sup>O crystals and how these two parameters determine the TE properties of the films. It is demonstrated that there is an optimal  $T_R$  value around 170 °C that helps reach the highest TE performances that are essentially determined by the level of in-plane orientation rather than the crystal contact plane of PBTTT-<sup>8</sup>O.

## 2. Results

### 2.1. Orientation, polymorphism and contact plane as a function of rubbing temperature $T_R$ in oriented PBTTT-<sup>8</sup>O

Before turning to the doped films of PBTTT-<sup>8</sup>O, we first investigated the microstructure of the films aligned by high- $T$  rubbing at different rubbing temperatures. Alignment of PSCs such as P3HT and PBTTT is readily obtained by using the method of high temperature rubbing.<sup>31,32</sup> A rotating cylinder is applied on a heated PSC thin film surface at a given temperature and pressure (Fig. 1a). Adjusting the temperature during film rubbing is essential as it helps modulate the thermomechanical properties of the PSC films. Melting the alkyl side chains of a PSC imparts higher mobility to the conjugated backbone that aligns more readily along the rubbing direction. For polymers such as P3HT or PBTTT, the rubbing temperature controls both film crystallinity and in-plane orientation.<sup>31,32,35</sup>  $T_R$  impacts the level of in-plane chain orientation that can be quantified by extracting the 3D order parameter OP from the dichroic ratio (DR) of the main absorption band of the aligned polymer thin films.<sup>31</sup> Fig. 2c shows the evolution of the orientation in PBTTT-<sup>8</sup>O films *versus*  $T_R$ . The dichroic ratio DR goes through a maximum for a rubbing temperature close to 170 °C with  $\text{DR} = 22$  corresponding to an order parameter  $\text{OP} = 0.86$  ( $\text{OP} = (\text{DR} - 1)/(\text{DR} + 2)$ ) (measured at the maximum of absorption in the range 525–540 nm). A progressive decrease of DR is observed beyond that temperature as  $T_R$  approaches the melting temperature ( $T_m = 250 \text{ °C}$ ). TEM ED shows that this reduction in DR coincides with the progressive change of the contact plane from face-on to edge-on (Fig. 3). Importantly, we observe a clear decrease in the OP for  $T_R \geq 230 \text{ °C}$  and for  $T_R = 240 \text{ °C}$  we obtain  $\text{OP} = 0.64$ . The fact that alignment tends to decrease beyond a given  $T_R$  is a general observation (also seen for P3HT).<sup>31,35</sup> As noted in our earlier work, the observed alignment depends on both  $T_R$  and the  $M_n$  distribution of the polymer.<sup>35</sup> We attribute the decrease in orientation for  $T_R > 170 \text{ °C}$  to the normal sample dispersity ( $M_n = 30 \text{ kDa}$



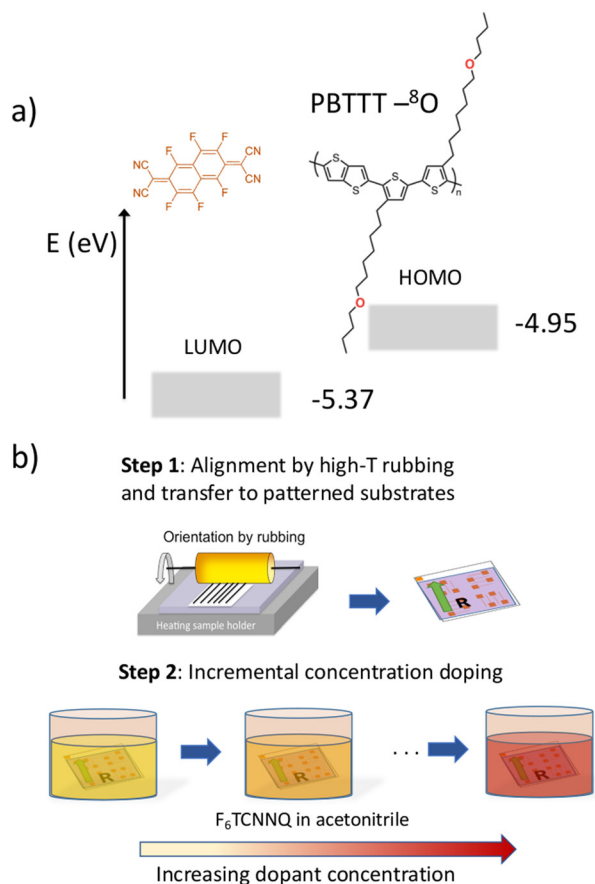


**Fig. 1** (a) Chemical structures of the polymer PBTTT-<sup>8</sup>O and the dopant F<sub>6</sub>TCNNQ and (b) method of alignment by high temperature rubbing and incremental concentration doping (ICD) used to prepare highly oriented PBTTT-<sup>8</sup>O thin films. The arrow noted R corresponds to the rubbing direction.

and  $\bar{D} = 1.8$ ). Polymer chains of increasing length require larger rubbing temperature to be aligned. When approaching the melting temperature, longer chains might align but not the short chains that are molten and lead to non-oriented fraction of PBTTT-<sup>8</sup>O in the films once cooled to RT. The fraction of such non-oriented and relaxed chains increases when  $T_R$  approaches the melting temperature whereby reducing the order parameter of the films.

Further changes in the structure of PBTTT-<sup>8</sup>O can also be evidenced by polarized UV-vis-NIR spectroscopy. In particular,  $T_R$  impacts the vibronic structure and the position of the absorption spectrum of PBTTT-<sup>8</sup>O.<sup>36</sup> For POL $\perp$ R, the absorption of the films corresponds essentially to amorphous and non-oriented PBTTT chains (see Fig. 2a and b showing the evolution of the UV-vis spectra with  $T_R$  for POL $\parallel$ R and POL $\perp$ R). Interestingly, when  $T_R$  increases between 80 °C and 180 °C, the absorption of amorphous PBTTT zones shifts to the blue from 517 nm to 485 nm whereas for  $T_R$  approaching 240 °C, it shifts back to 510 nm. For POL $\parallel$ R, the vibronic structure of the spectra changes slightly with  $T_R$ . The 0-0 vibronic component is seen as a shoulder at 590 nm. It increases in intensity when increasing  $T_R$  between 80 °C and 180 °C and decreases substantially for higher  $T_R$  approaching 240 °C.

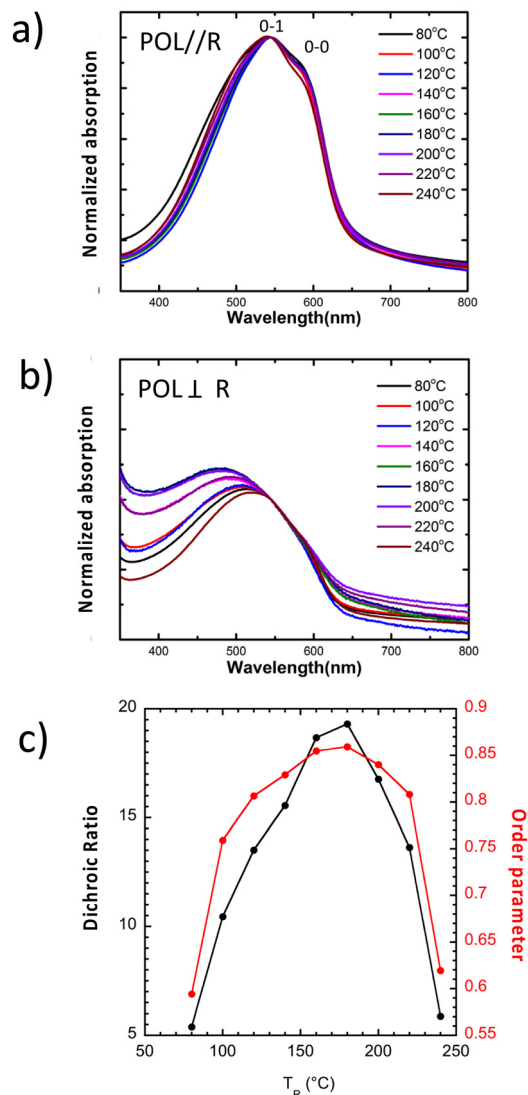


**Fig. 2** Evolution of the normalized UV-vis-NIR spectrum for POL $\parallel$ R (a) and POL $\perp$ R (b) as a function of the rubbing temperature for aligned PBTTT-<sup>8</sup>O films. (c) Dichroic ratio DR measured at 540 nm (black dots) and corresponding order parameter (red dots) defined as  $(DR - 1)/(DR + 2)$  as a function of the rubbing temperature  $T_R$  for thin films of PBTTT-<sup>8</sup>O.

For polythiophenes such as P3HT, the intensity of the 0-0 vibronic contribution is related to the extension of planarized chain segments in the crystals: the 0-0 component shows enhanced intensity when the planarized chain segment increases.<sup>31,36</sup> This result suggests chain segment planarization is enhanced around 180 °C in PBTTT-<sup>8</sup>O, in perfect agreement with the observed maximum of order parameter and charge conductivity in the doped films. Accordingly, the rubbed films of PBTTT-<sup>8</sup>O show a marked improvement of in-plane orientation and chain planarization around 180 °C which is of importance for the TE properties as shown hereafter.

The rubbing temperature  $T_R$  is also a handle to modify the structure of the aligned thin films *i.e.* contact plane and crystal dimensions.<sup>31</sup> As noted in our previous work, there is evidence for polymorphism in rubbed PBTTT-<sup>8</sup>O films. It is manifested



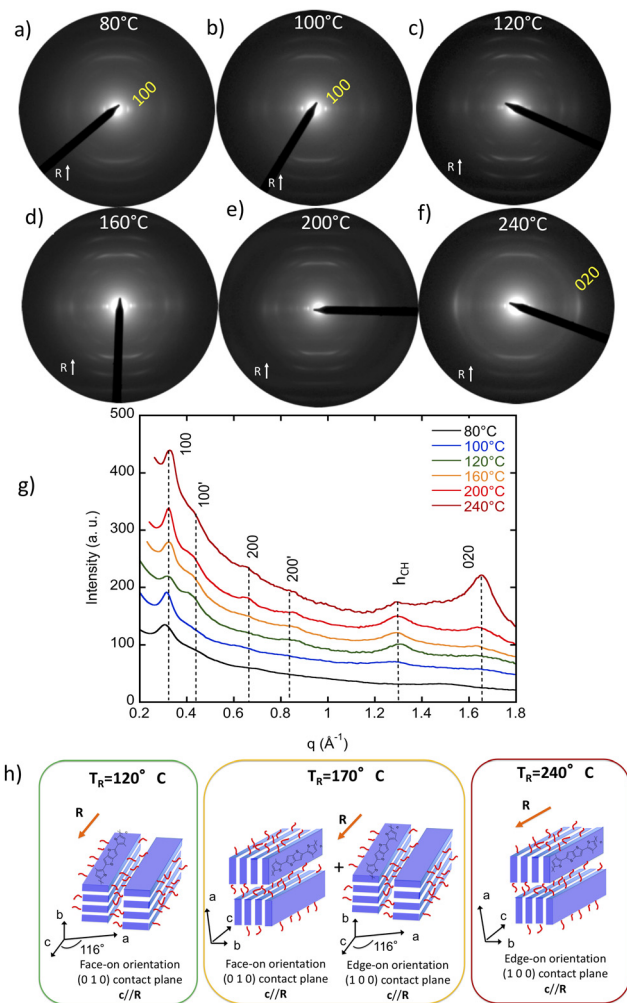


**Fig. 3** (a)–(f) Evolution of the electron diffraction pattern of PBTTT-<sup>8</sup>O thin films rubbed at different temperatures (rubbing direction is vertical). (g) Equatorial plot profile of the ED patterns as a function of  $T_R$ .  $h_{CH}$  originates from the scattering of  $C_7O_4$  side chains. (h) Schematic illustration of the dominant PBTTT-<sup>8</sup>O crystal contact plane in rubbed thin films as a function of  $T_R$ . For all  $T_R$ , the PBTTT-<sup>8</sup>O chains orient parallel to the rubbing direction  $R$  but the highest orientation is observed for  $T_R = 170$  °C. For  $T_R = 170$  °C, the film consists of a mixture of face-on and edge-on crystals.

by the coexistence of two lamellar reflections  $d_{100}$  and  $d_{100'}$  at 19.7 Å and 14.6–15.0 Å, respectively. The polymorph with the larger  $d_{100}$  is dominant regardless of  $T_R$  and  $d_{100}$  is close to the value found for PBTTT- $C_{12}$ . The section profile of the ED patterns in Fig. 3g suggests that the proportion of the 14.6–15.0 Å polymorph is most pronounced for  $T_R = 120$  °C and tends to decrease at larger  $T_R$ .

This polymorph is possibly related to a structure with more tilted side chains and such polymorphism has been observed in the family of poly(alkylthiophene)s.<sup>37</sup> It may correspond to a side chain conformation that is formed predominantly around  $T_R = 120$  °C because of the presence of the ether group that is expected to modify its conformation as compared to a linear  $C_{12}$  side chain. Indeed, due to the presence of the ether function, a significant increase of gauche effects, which lead to

coil/random side chains, are expected for PBTTT-<sup>8</sup>O as regards to the usual PBTTT- $C_{12}$ .<sup>38</sup> The majority of the reflections in the ED patterns for  $T_R = 120$  °C and 160 °C are attributed to the dominant polymorph with  $d_{100} = 19.7$  Å.

As shown in our previous work, the reflections of this polymorph for  $T_R = 170$  °C can be indexed using a monoclinic unit cell with  $a = 21.9$  Å,  $b = 7.6$  Å,  $c = 13.7$  Å and  $\beta = 116^\circ$ . Modeling of the structure was performed to calculate ED patterns and compare them with the experimental ED pattern (see Fig. 4). To ease the structural refinement, we considered that side chains are ordered (DSC on powdered samples suggested that they are rather disordered, see ref. 12). The refined model involves a monoclinic unit cell with two chains per unit cell and  $P\bar{1}$  space group (see Fig. 4d and e). The off-meridional position of the most intense  $-3\ 0\ 3$  reflection is the signature of this structure and it reflects the fact that side chains, although partially disordered, are tilted to the PBTTT backbone and located within the  $-3\ 0\ 3$  planes. This is at variance with PBTTT- $C_{12}$  for which the predominant meridional position of the  $0\ 0\ 3$  reflection (see Fig. S1, ESI†) indicates that the side chains are located in a plane perpendicular to the PBTTT backbone. The consequence of tilted  $C_7$ – $O$ – $C_4$  side chains is that the successive PBTTT  $\pi$ -stacks are offset along the chain direction in the monoclinic unit cell of PBTTT-<sup>8</sup>O as compared to PBTTT- $C_{12}$ . Accordingly, the introduction of an ether function in the side chain modifies the packing of successive layers of  $\pi$ -stacked PBTTT backbones. Incidentally, the refined structure of PBTTT-<sup>8</sup>O suggests that oxygen atoms of the ether are located within a common plane inside the side chain layers, which may explain to some extent the higher side chain cohesion evidenced by DSC.<sup>16</sup> This explains at least in part the better thermomechanical properties of PBTTT-<sup>8</sup>O that can be aligned up to very high temperatures close to the melting, contrary to PBTTT- $C_{12}$ .

Changes of the contact plane induced by the rubbing temperature are best visualized by plotting the equatorial section profiles of the ED patterns as a function of increasing rubbing temperature and comparing the relative intensities of the  $h\ 0\ 0$  ( $h = 1$ –3) and  $0\ 2\ 0$  reflections (see Fig. 3). For  $T_R \leq 120$  °C, the intensity of the equatorial  $0\ 2\ 0$  is very small and the intensities of the  $h\ 0\ 0$  ( $h = 1, 2$  and 4) are by far dominating. Thus, films formed at  $T_R \leq 120$  °C are essentially made of face-on oriented PBTTT-<sup>8</sup>O crystals. For  $T_R \geq 200$  °C, the situation changes progressively with a strong increase of the intensity of the  $0\ 2\ 0$  reflection that is dominant for  $T_R = 240$  °C. Accordingly, films rubbed at 240 °C are essentially made of edge-on oriented crystals. The films prepared at  $T_R = 170$  °C are composed of a mixture of edge-on and face-on crystals with a predominance of the latter. Thus, by changing  $T_R$  it is possible to probe if the proportion of face-on/edge-on crystals impacts or not the TE properties of doped PBTTT-<sup>8</sup>O films.

## 2.2 Influence of the PBTTT-<sup>8</sup>O structure on the spectroscopic signatures of $F_6TCNNQ^-$ anions in the oriented thin films

Having demonstrated that rubbing temperature determines in-plane orientation and structure of PBTTT-<sup>8</sup>O thin films, we





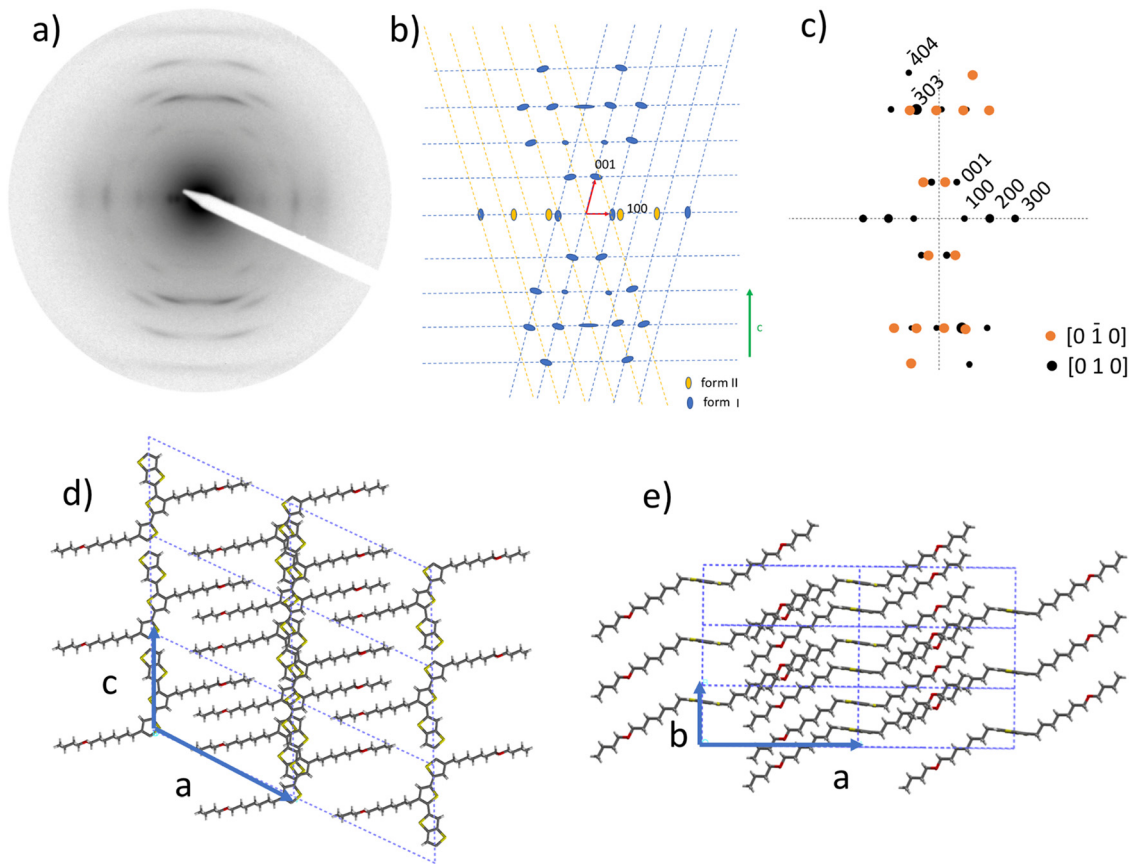


Fig. 4 (a) Electron diffraction pattern of an oriented PBTTT-<sup>8</sup>O film aligned by high-*T* rubbing at  $T_R = 170^\circ\text{C}$ . (b) Schematic representation of the ED pattern, (c) calculated ED pattern in black for a monoclinic unit cell with [010] (black) and [0  $\bar{1}$  0] zone axes. *b*-Axis (d) and *c*-axis (e) projections of the refined structure of PBTTT-<sup>8</sup>O.

have followed the doping of oriented thin films using polarized UV-vis-NIR spectroscopy. We have chosen three conditions:  $T_R = 120^\circ\text{C}$  for mainly face-on oriented films,  $T_R = 170^\circ\text{C}$  corresponding to a mixture of edge-on/face-on crystals with maximum in-plane orientation and  $T_R = 240^\circ\text{C}$  for aligned films made of edge-on crystals (see Fig. S2, ESI†). For these three films, we have followed the evolution of the UV-vis-NIR spectra *versus* F<sub>6</sub>TCNNQ concentration in acetonitrile (Fig. 5). The advantage of using polarized light is that we can distinguish different contributions in the spectra such as oriented and ordered PBTTT-<sup>8</sup>O domains (POL||R) or amorphous PBTTT-<sup>8</sup>O domains (POL⊥R).

Regarding the spectra at  $T_R = 120^\circ\text{C}$ , the evolution as a function of increasing dopant concentration for POL⊥R is interesting. Indeed, for  $[\text{F}_6\text{TCNNQ}^-] \leq 0.1 \text{ g l}^{-1}$ , the vibronic structure corresponding to the F<sub>6</sub>TCNNQ<sup>−</sup> anion is well observed with three components corresponding to 0–0, 0–1 and 0–2 contributions. For  $[\text{F}_6\text{TCNNQ}^-] \geq 0.5 \text{ g l}^{-1}$ , the situation changes and beside the anion vibronic structure, a broad band around 800 nm that overlaps with the 0–2 of the F<sub>6</sub>TCNNQ<sup>−</sup> anion appears and tends to gain in intensity with increasing dopant concentration. In our previous work, this band was attributed to dimers of F<sub>6</sub>TCNNQ<sup>−</sup>, in agreement with earlier results on (TCNQ<sup>−</sup>)<sub>2</sub> dimers as well as clustering of

F<sub>6</sub>TCNNQ probed by electron paramagnetic resonance.<sup>39,40</sup> The fact that the broad band at 800 nm appears only at larger dopant concentration is fully consistent with its attribution to dimers (F<sub>6</sub>TCNNQ<sup>−</sup>)<sub>2</sub> since the probability to form them should increase with the dopant concentration in PBTTT-<sup>8</sup>O. Interestingly, the same trend *i.e.* a gradual increase of the dimer band at 800 nm with increasing doping concentration is also seen for the films prepared at  $170^\circ\text{C}$  and  $240^\circ\text{C}$ . It is worth to recall that for PBTTT-C<sub>12</sub>, no such dimer band was evidenced in the same range of [F<sub>6</sub>TCNNQ], indicating that the formation of such dimers is favored by the presence of C<sub>7</sub>–O–C<sub>4</sub> side chains in PBTTT-<sup>8</sup>O.

Notably, it is possible to compare the films grown at various  $T_R$  in terms of dimer concentration. As seen in Fig. 5, when considering the highest [F<sub>6</sub>TCNNQ] of  $5 \text{ g l}^{-1}$ , there is a clear trend in the ratio of the dimer band *versus* 0–0 F<sub>6</sub>TCNNQ<sup>−</sup> band when the rubbing temperature is increasing. At  $120^\circ\text{C}$ , the 0–0 contribution of F<sub>6</sub>TCNNQ<sup>−</sup> absorption is of lower intensity than the dimer band. For  $T_R \geq 170^\circ\text{C}$ , the trend is reversed, the 0–0 band becomes more intense. This observation indicates that the dimer/anion ratio in the F<sub>6</sub>TCNNQ-doped PBTTT-<sup>8</sup>O films changes with the structure of the films. As observed by TEM ED, the films grown at  $T_R \geq 170^\circ\text{C}$  show more mixed index reflections, suggesting that the films are



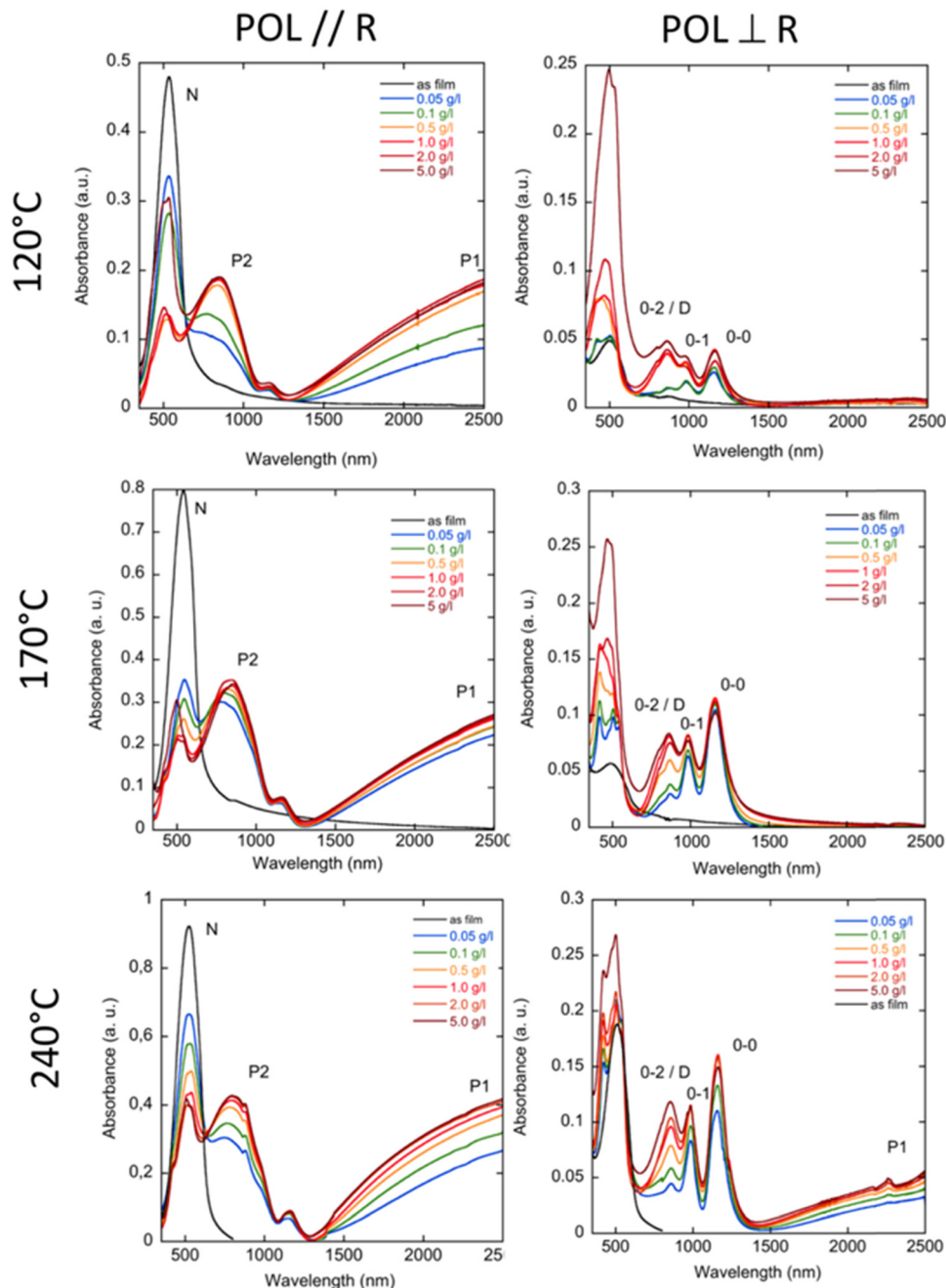


Fig. 5 Evolution of the UV-vis-NIR spectrum of PBTTT-<sup>8</sup>O thin films as a function of the doping concentration with F<sub>6</sub>TCNNQ and for three films oriented by rubbing at 120 °C, 170 °C and 240 °C. The figures in the left column correspond to the spectra recorded for a light polarization POL||R (R is the rubbing direction) whereas for the right column, POL⊥R. The broad absorption band near 800 nm that overlaps with the 0–2 band of the radical anion F<sub>6</sub>TCNNQ<sup>•−</sup> is attributed to dimers of the dopant anion F<sub>6</sub>TCNNQ<sup>•−</sup> and noted as D.<sup>39,40</sup>

more ordered and in particular the packing of C<sub>7</sub>–O–C<sub>4</sub> chains is possibly more ordered than for  $T_R = 120$  °C. This is why we propose that the disorder in the C<sub>7</sub>–O–C<sub>4</sub> side chains modulates the formation of F<sub>6</sub>TCNNQ<sup>•−</sup> dimers: a higher level of disorder in the side chain packing favors the formation of dimers.

It is worth to note that similar spectroscopic signatures of dimer-like features were observed in F<sub>4</sub>TCNQ-doped P3HT films and attributed to the Charge Transfer Complex (CTC)

between P3HT and F<sub>4</sub>TCNQ.<sup>41</sup> The comparison with the present work and with ref. 41 suggests that the observed bands around 800 nm previously assigned to CTC correspond rather to dimers of the sole dopant radical anions F<sub>4</sub>TCNQ<sup>•−</sup>.

For POL||R, regarding the polaronic bands P1 and P2, a clear evolution with the dopant concentration and with the rubbing temperature is observed. In the PBTTT-<sup>8</sup>O films rubbed at 170 °C, the P2 band is redshifted from 790 nm at 0.05 g l<sup>−1</sup> to 858 nm at 5 g l<sup>−1</sup>. This suggests that the polarons should be



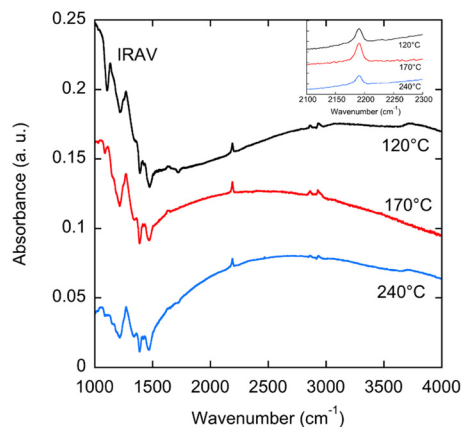


Fig. 6 Evolution of the normalized IR spectrum of PBTTT-<sup>8</sup>O thin films oriented at different rubbing temperatures and doped by ICD using F<sub>6</sub>TCNNQ in ACN (1 g l<sup>-1</sup>). Infrared-active vibrational (IRAV) modes are highlighted. The inset shows the expanded view of the FTIR spectrum around C≡N stretching peak of the dopant anion F<sub>6</sub>TCNNQ<sup>•-</sup>.

more delocalized with increasing dopant concentration and it illustrates the fact that the local environment of the polarons changes with dopant concentration. The same type of P2 band shift is also observed for the films prepared at 120 °C and 240 °C. However, for  $T_R = 240$  °C, the P2 band shifts to 797 nm at 5 g l<sup>-1</sup>. In other words, the P2 band is substantially more redshifted for  $T_R = 170$  °C than for  $T_R = 240$  °C, which suggests that the polarons are better delocalized as compared to the films prepared at 120 °C and 240 °C.<sup>9,10</sup> A close look at the P1 band *versus*  $T_R$  using FTIR spectroscopy confirms the previous observations for the P2 band. As seen in Fig. 6, the P1 band seems more red-shifted for  $T_R = 170$  °C than for  $T_R = 120$  °C and 240 °C. In addition, the FTIR spectra also show the typical C≡N stretching peak of the F<sub>6</sub>TCNNQ<sup>-</sup> anions at 2190 cm<sup>-1</sup>. Notably, no trace of the neutral F<sub>6</sub>TCNNQ dopant is observed at 2213 cm<sup>-1</sup> for films doped at 1 g l<sup>-1</sup> indicating that the majority of dopant molecules are ionized in the oriented PBTTT-<sup>8</sup>O films.<sup>34</sup>

### 2.3 Structural evolution in oriented PBTTT-<sup>8</sup>O films *versus* doping

The evolution of the structure with increasing dopant concentration was followed for the three thin films aligned at 120 °C, 170 °C and 240 °C using electron diffraction. Fig. 7 exemplifies the variation of the lattice parameters corresponding to the lamellar periodicity along the side chains  $d_{100}$  and the  $\pi$ -stacking periodicity  $d_{020}$  as a function of increasing concentration of F<sub>6</sub>TCNNQ. For PBTTT with C<sub>12</sub> alkyl side chains, doping with F<sub>6</sub>TCNNQ results in a small increase of  $d_{100}$  from 19.7 Å to 20.3 Å and a decrease of the  $\pi$ -stacking distance from 3.8 Å to 3.65 Å.<sup>24,31</sup> For all rubbing temperatures, a different behavior is observed in the case of PBTTT-<sup>8</sup>O. For [F<sub>6</sub>TCNNQ] ≤ 0.5 g l<sup>-1</sup>,  $d_{100}$  tends to increase and  $d_{020}$  to decrease. This suggests that the PBTTT-<sup>8</sup>O lattice can accommodate a small amount of F<sub>6</sub>TCNNQ dopant in its lattice. However, beyond this concentration, a reverse trend is observed with a reduction of

$d_{100}$  and an increase of  $d_{020}$  for  $T_R = 120$  °C and 170 °C. Notably, for  $T_R = 170$  °C, the final values of  $d_{100}$  and  $d_{020}$  for [F<sub>6</sub>TCNNQ] = 5 g l<sup>-1</sup> are almost identical to the values of the pristine PBTTT-<sup>8</sup>O. In our previous study, polarized UV-vis-NIR spectroscopy and EPR showed that the orientation of F<sub>6</sub>TCNNQ in PBTTT-<sup>8</sup>O grown at  $T_R = 170$  °C is random inside the side chain layers of PBTTT-<sup>8</sup>O, in strong contrast to PBTTT-C<sub>12</sub> for which the dopants orient very well in the direction perpendicular to the alkyl side chains.<sup>16,33</sup> The abnormal dependence of PBTTT-<sup>8</sup>O lattice parameters with increasing dopant concentration [F<sub>6</sub>TCNNQ] indicates some kind of re-organization of the lattice upon dopant incorporation. At a larger [F<sub>6</sub>TCNNQ], dopants are expected to interact more together inside the disordered side chain layers of C<sub>7</sub>-O-C<sub>4</sub> and to cluster (see Fig. 7e). Our results suggest that the dopant's reorientation/reorganization in the side chain layers is a consequence of dopant anion's clustering and that this phenomenon depends on the order initially present in the side chain layers. Clustering seems more favorable when C<sub>7</sub>-O-C<sub>4</sub> side chain layers are more disordered ( $T_R \leq 120$  °C). It is also worth to mention that preferential location of dopant molecules in the only amorphous phase of PBTTT-<sup>8</sup>O, as observed for magic blue in semi-crystalline P3HT seems unlikely for PBTTT-<sup>8</sup>O. Indeed, for P3HT doped with MB, lattice parameters are unchanged whatever the MB dopant concentration, contrary to PBTTT-<sup>8</sup>O doped with F<sub>6</sub>TCNNQ.<sup>42</sup> Moreover, polarized UV-vis-NIR spectroscopy measurements in Fig. 5 show that, similarly to PBTTT-C<sub>12</sub>, the amorphous phase of PBTTT-<sup>8</sup>O is not doped by F<sub>6</sub>TCNNQ (no bleaching of the neutral amorphous polymer band).<sup>42</sup> This is in contrast to FeCl<sub>3</sub> that can dope both crystalline and amorphous PBTTT-<sup>8</sup>O phases. It is therefore instructive to compare the structural variation upon doping observed for F<sub>6</sub>TCNNQ with that for FeCl<sub>3</sub>-doped films (see Fig. S3 and Fig. 7d). Indeed, contrary to F<sub>6</sub>TCNNQ-doping, a very different situation is observed when the PBTTT-<sup>8</sup>O films are doped with FeCl<sub>3</sub> (see Fig. 7d). In that case,  $d_{100}$  increases steadily up to 24.0 Å at [FeCl<sub>3</sub>] = 5 g l<sup>-1</sup> in the same way as observed previously for PBTTT-C<sub>12</sub> doped with FeCl<sub>3</sub>. However, in strong contrast to doping with F<sub>6</sub>TCNNQ, doping PBTTT-<sup>8</sup>O with FeCl<sub>3</sub> results in a total loss of reflections corresponding to order in the chain direction for [FeCl<sub>3</sub>] = 5 g l<sup>-1</sup>. In other words, stacking order within  $\pi$ -stacks is strongly altered in PBTTT-<sup>8</sup>O at high concentration of FeCl<sub>3</sub> and more preserved in the case of F<sub>6</sub>TCNNQ doping. This explains, at least in part, the reduced TE properties measured for FeCl<sub>3</sub>-doped films as compared to F<sub>6</sub>TCNNQ (see next section).

### 2.4 Anisotropic TE properties *versus* rubbing temperature

Finally, we measured the anisotropic TE performances of the doped and oriented PBTTT-<sup>8</sup>O films for the three selected  $T_R$  of 120 °C, 170 °C and 240 °C in the directions parallel and perpendicular to the rubbing (see Table 1 and Fig. 8). For all films, a marked anisotropy of TE properties is observed in the oriented films. The anisotropy of charge conductivity is in the range 3.4–29. It is most pronounced for the films prepared at  $T_R = 170$  °C, in agreement with the higher DR observed at this  $T_R$ .



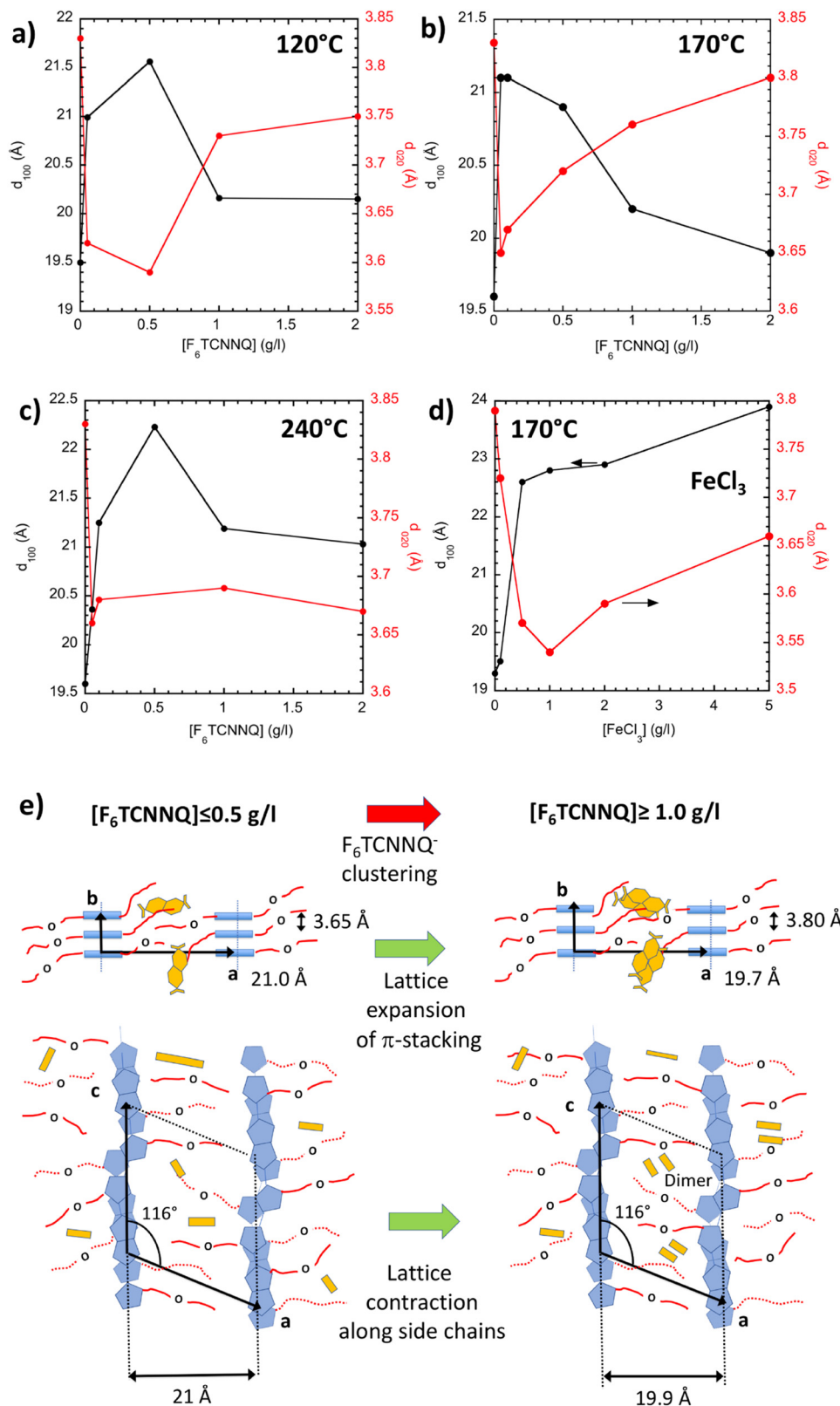


**Fig. 7** (a–c) Evolution of the reticular distance  $d_{100}$  and  $d_{020}$  corresponding the lamellar period and the  $\pi$ -stacking periodicity as a function of F<sub>6</sub>TCNNQ concentration in acetonitrile for PBTTT-<sup>8</sup>O thin films aligned by high- $T$  rubbing at 120 °C (a), 170 °C (b) and 240 °C (c). For comparison, we show in (d) the evolution of the same lattice parameters of PBTTT-<sup>8</sup>O with increasing concentration of FeCl<sub>3</sub> ( $T_R$  = 170 °C). (e) Schematic illustration of the structural changes in PBTTT-<sup>8</sup>O induced by the clustering of F<sub>6</sub>TCNNQ<sup>•+</sup> upon increasing doping concentration.





**Table 1** Maximum anisotropy coefficients of oriented PBTTT-<sup>8</sup>O thin films doped with F<sub>6</sub>TCNNQ and aligned by high-*T* rubbing at different temperatures *T<sub>R</sub>*

<i>T<sub>R</sub></i>	Dichroic ratio	3D order parameter	Ratio P1/neutral	Maximum conductivity $\sigma_{  }$ (S cm <sup>-1</sup> )	Charge conductivity anisotropy $\sigma_{  }/\sigma_{\perp}$	Seebeck coefficient anisotropy $S_{  }/S_{\perp}$	Maximum power factor ( $\mu\text{W m}^{-1} \text{K}^{-2}$ )
120 °C	13.5	0.8	0.38	3250	4.7	4.2	256
170 °C	19.3	0.87	0.34	$2-5 \times 10^4$	29	4.3	1000–2900
240 °C	5.9	0.62	0.43	1100	3.4	3.0	16
FeCl <sub>3</sub> 170 °C	19.3	0.87	—	9500	21	4.7	100

As reported previously, the films grown at *T<sub>R</sub>* = 170 °C show a very high charge conductivity in the range  $2-5 \times 10^4 \text{ S cm}^{-1}$  in the direction parallel to the rubbing. Even for a high dopant concentration of  $5 \text{ g l}^{-1}$ , there is no true saturation of the conductivity but larger concentrations of F<sub>6</sub>TCNNQ are prohibited by the solubility limit of F<sub>6</sub>TCNNQ in ACN. As a means of comparison, FeCl<sub>3</sub>-doped PBTTT-<sup>8</sup>O films prepared at 170 °C yield charge conductivities  $\sigma_{||}$  up to  $9500 \pm 3000 \text{ S cm}^{-1}$  (for  $5 \text{ g l}^{-1}$ , see Fig. S4, ESI†). This value is significantly below  $2-5 \times 10^4 \text{ S cm}^{-1}$  obtained for F<sub>6</sub>TCNNQ-doped PBTTT-<sup>8</sup>O. This lower conductivity coincides with the strongly reduced order in the FeCl<sub>3</sub>-doped PBTTT-<sup>8</sup>O films as evidenced by TEM (see Fig. S3, ESI†) and supports the idea that introduction of dopants in the polymer host must preserve to the extent possible the original structure of the PBTTT-<sup>8</sup>O crystals.

Concerning the rubbing temperature, it has a drastic impact on the TE performances of the F<sub>6</sub>TCNNQ-doped PBTTT-<sup>8</sup>O. Both the PBTTT-<sup>8</sup>O films prepared at 120 °C and 240 °C show a much smaller charge conductivity  $\sigma_{||}$  of  $3250 \text{ S cm}^{-1}$  and  $1100 \text{ S cm}^{-1}$ , respectively, for  $[\text{F}_6\text{TCNNQ}] = 5 \text{ g l}^{-1}$ . Notably, the conductivity at *T<sub>R</sub>* = 240 °C is similar to that of non-oriented thin films which is consistent with the low alignment level achieved at 240 °C *i.e.* OP = 0.62 (see Table 1). As a remark, these differences in charge conductivity are not related to strong differences in doping levels. The doping level can be tentatively approximated by the ratio of the P1 band absorbance at 2500 nm and the absorbance of the undoped polymer film (for parallel orientation).<sup>20</sup> As seen in Table 1, the three films show similar values of this ratio in the 0.34–0.43 range, indicating that the observed charge transport differences must be due to differences in charge mobilities.

Regarding the Seebeck coefficient, it is larger when measured in the direction of chain alignment than perpendicular, but the observed anisotropy is substantially lower than for charge conductivity,  $S_{||}/S_{\perp}$  is in the range 3–4. Overall, the results are consistent with the differences in structure and alignment of the three films and they underline the beneficial role of orientation on the thermopower *S*.<sup>19</sup> The highest conductivity is expectedly observed for the film that displays the best in-plane orientation and also the most extended planarized chain segments *i.e.* for *T<sub>R</sub>* = 170 °C and therefore a clear correlation between in-plane orientation and  $\sigma_{||}$  is observed. The importance of in-plane orientation is predominant over other parameters and minor variations in the OP have a major impact on the charge conductivity in the chain direction. This is somehow expected from the theoretical work of Ihnatsenka

*et al.* indicating that  $\sigma_{||}/\sigma_{\perp}$  increases exponentially with the order parameter.<sup>19</sup> Regarding the anisotropy in Seebeck coefficients, it has been shown that it can be explained if anisotropic long-range repulsive Coulombic interactions between carriers are taken into account in the hopping between localized states. In particular, a stronger screening of Coulomb interactions in the direction parallel to the chains with respect to perpendicular direction can explain the strong anisotropy of *S* whereas the use of only on-site Coulomb interactions cannot capture this effect.<sup>19,43</sup> For the range of very high charge conductivities ( $>10^4 \text{ S cm}^{-1}$ ) for *T<sub>R</sub>* = 170 °C, the hopping regime might not be appropriate to describe transport properties. In that case, it might be the stronger delocalization of carriers due to enhanced chain segment planarization of PBTTT-<sup>8</sup>O that could explain a stronger screening of Coulomb interactions in the chain direction, hence the anisotropy of the Seebeck coefficient.

Notably, the best Power factors for the doped PBTTT-<sup>8</sup>O films are obtained for the films prepared at 170 °C and doped at  $2 \text{ g l}^{-1}$  *i.e.* showing a structure close to that of the pristine undoped films prior to doping. PF reaches values in the range 1000–2900  $\mu\text{W m}^{-1} \text{K}^{-2}$ . The films of PBTTT-<sup>8</sup>O prepared at 120 °C and 240 °C the lattice of which is most altered upon doping show reduced TE performances with PF in the range 16–256  $\mu\text{W m}^{-1} \text{K}^{-2}$  *i.e.* comparable to 100  $\mu\text{W m}^{-1} \text{K}^{-2}$  observed for FeCl<sub>3</sub>-doped films. This observation supports the idea that high TE performances can only be observed when (i) high in-plane orientation of the PBTTT chains is obtained by rubbing prior to doping and (ii) the structure of the doped material remains close to that of the undoped pristine polymer. Overall, these conclusions are in line with the recent work of Jacobs *et al.* on the influence of *para*-crystallinity measured in the  $\pi$ -stacking direction on the charge transport properties in doped polymer semiconductors.<sup>44</sup> As a side remark, the polymorphism of PBTTT-<sup>8</sup>O evidenced in the pristine films seems to have little influence on the TE performances of doped films.

Finally, we investigated the *S*– $\sigma$  correlations in the oriented PBTTT thin films that can help analyze transport phenomena in doped PSCs.<sup>45</sup> For PBTTT-C<sub>12</sub>, we have demonstrated two different scaling laws in the directions parallel and perpendicular to the chain orientation, regardless of the type of dopant used (FeCl<sub>3</sub>, F<sub>4</sub>TCNQ and F<sub>6</sub>TCNNQ).<sup>22,42</sup> In the chain direction, a power law of the type  $S_{||} \propto \sigma_{||}^{-1/4}$  was evidenced and a different relation of the type  $S_{\perp} \propto -\log(\sigma_{\perp})$  perpendicular to the chains.<sup>22</sup> The power law dependence with an exponent  $s = -1/4$  has been predicted by different models.<sup>46–49</sup> Kemerink and coworkers proposed that variable range hopping transport



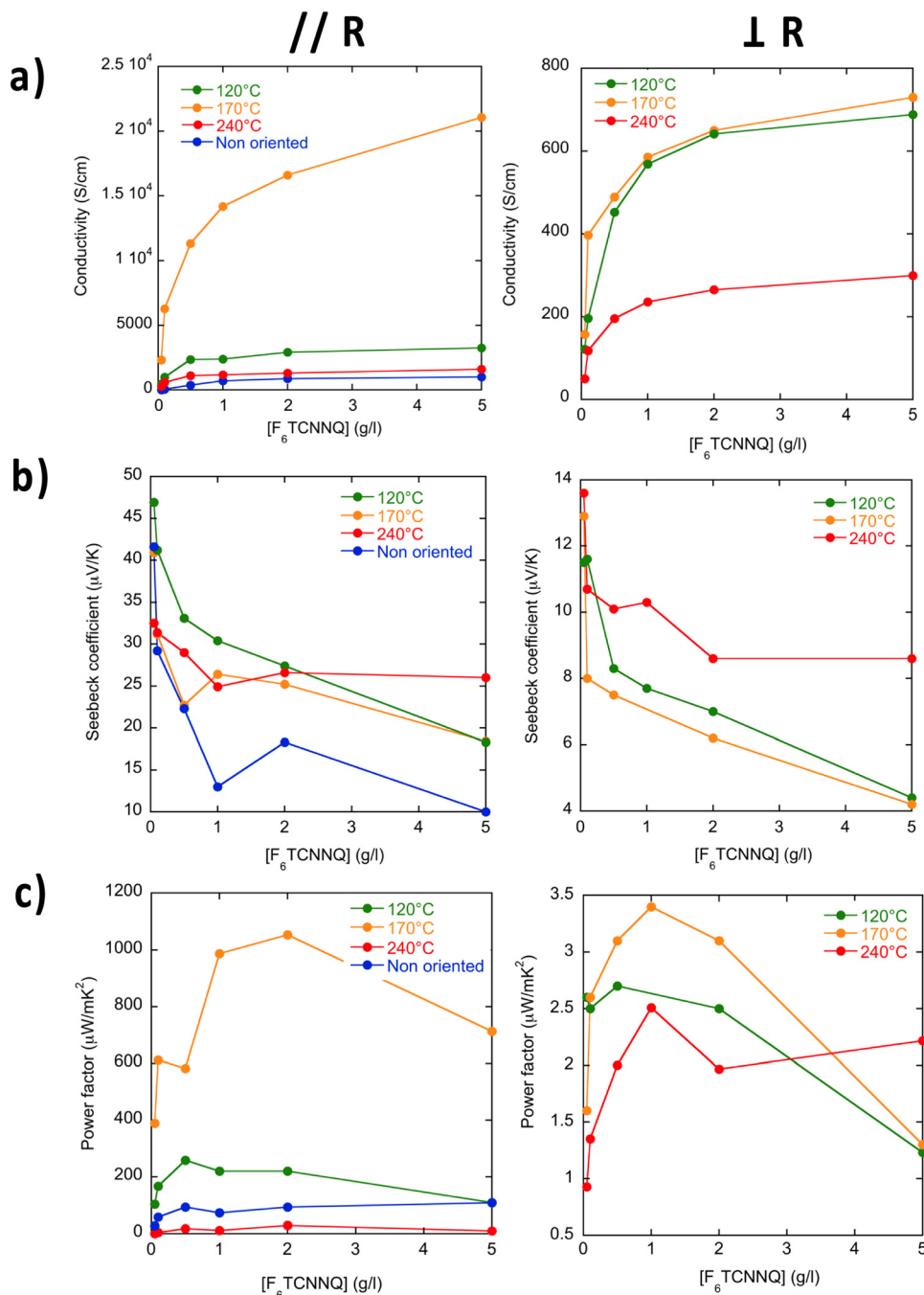


**Fig. 8** Evolution of the charge conductivity (a), the Seebeck coefficient (b) and the thermoelectric power factor (c) as a function of the dopant concentration of  $F_6TCNNQ$  in the directions parallel and perpendicular to the rubbing for aligned PBTTT-<sup>8</sup>O thin films rubbed at different temperatures. Data for a non-oriented PBTTT-<sup>8</sup>O thin film are provided for comparison.

in a system with a gaussian DOS and Coulomb trapping by ionized dopants can account for this type of correlation. However, such a model can only apply over a limited range of conductivities and can hardly be extrapolated to the range of conductivities  $>1000$  S cm<sup>-1</sup>.<sup>43,46</sup> Limelette and coworkers used a different approach considering rather delocalized carriers such as Dirac fermions with a parabolic DOS and a scattering mechanism by unscreened charged impurities.<sup>47</sup> More recently, Gregory *et al.* proposed an improved version of

the Kang and Snyder transport model *i.e.* a semi-localized transport (SLoT) model to bridge the gap between localized and delocalized transport in conducting polymers.<sup>48,49</sup>

In Fig. 9, we have merged the  $S$ ,  $\sigma$  data points relative to the PBTTT-<sup>8</sup>O film oriented at 170 °C and doped with solutions of  $F_6TCNNQ$  of different concentrations along with the data obtained for PBTTT-C<sub>12</sub> doped with various dopants ( $FeCl_3$ ,  $F_4TCNNQ$ ,  $F_6TCNNQ$ ). Most interestingly, the data points for the polymer with single ether C<sub>7</sub>OC<sub>4</sub> side chains oriented at 170 °C



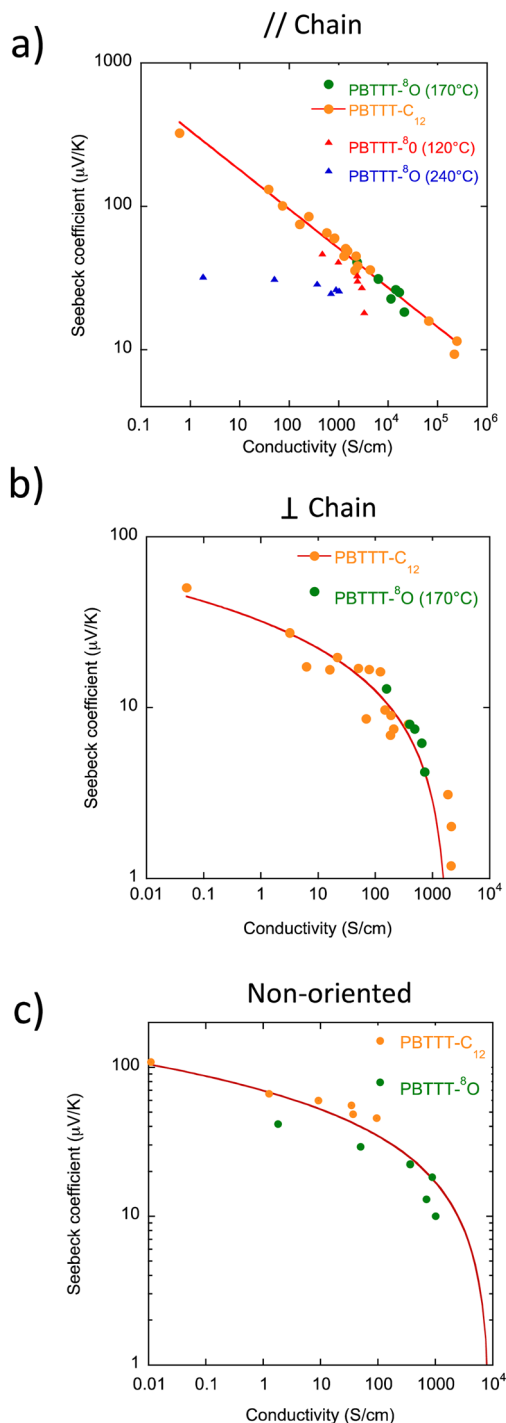


**Fig. 9** Correlations between the Seebeck coefficient and charge conductivity measured in the direction parallel (a) and perpendicular (b) to the rubbing direction for PBTTT- $C_{12}$  and PBTTT- $^8O$  films rubbed at 125 °C and 170 °C, respectively. The continuous lines correspond to the fits with a power law ( $\parallel$ ) and a logarithmic relation ( $\perp$ ). (c) Correlations between the Seebeck coefficient and charge conductivity measured in non-oriented thin films of PBTTT- $C_{12}$  and PBTTT- $^8O$ .

fall onto the same master curves obtained previously for PBTTT- $C_{12}$  for both directions  $\parallel$  and  $\perp$  to the rubbing. In strong contrast, the data points obtained for the films oriented at 120 °C and

240 °C do not comply with the trends of the master curves. In particular, the poor alignment of the PBTTT- $^8O$  films for  $T_R = 120$  °C and 240 °C results in totally different  $S$ - $\sigma$  correlation curves closer to the non-oriented films and far away from the power law relation seen in the chain direction (see Fig. 9a). This result suggests that the PBTTT backbone, its in-plane orientation and  $\pi$ -stacking rather than the chemical natures of the side chains and dopant determines the type of  $S$ - $\sigma$  scaling observed in the oriented PBTTT *i.e.* the anisotropic charge transport at play. It also suggests that neither the presence of polymorphism, nor the presence of dimers of  $F_6TCNNQ^{\bullet-}$  in PBTTT- $^8O$  thin films impacts negatively the TE performances. Conversely, poor in-plane orientation observed for  $T_R = 120$  °C and 240 °C and perturbation of  $\pi$ -stacking within individual PBTTT  $\pi$ -stacks modifies substantially the  $S$ - $\sigma$  correlations. This result is important in the sense that anisotropic charge transport mechanism at play in oriented doped PSCs is primarily determined by structure and orientation control while the chemical nature of dopant and side chains seem more secondary factors in determining the upper limits of TE performances. These parameters become probably predominant for other aspects such as long-term stability of the doped systems or processing of thin films. Indeed, engineering of PSC side chains and of the dopant plays a primary role in the processing of polymer and dopant or long-term stability of the doped PSCs.<sup>50</sup>

The  $S$ - $\sigma$  correlation in non-oriented films is very close to that for the films measured in the direction perpendicular to the chains with a logarithmic dependence. This result underlines the importance to measure the  $S$ - $\sigma$  correlations in oriented films since the retained model (for instance the Kang-Snyder or the semi-localized transport model by Gregory *et al.*)<sup>48,49</sup> to adjust the  $S$ - $\sigma$  relationships in non-oriented samples is not representative of charge transport in the chain direction but may be dominated by transport in the direction perpendicular to the chains. Accordingly, applying transport models such as SLoT to non-oriented polymer films will inherently account for variable proportions of the intra-chain (delocalized) and inter-chain (localized) transport.

### III. Conclusion

The anisotropic TE properties of PBTTT- $^8O$  thin films aligned by high- $T$  rubbing and doped with  $F_6TCNNQ$  have been studied. The rubbing temperature is a handle to control in-plane chain orientation of PBTTT backbones and the crystal's contact plane on the substrate.  $T_R$  is a key parameter controlling the final TE performances of the aligned films. An optimum in TE performances corresponding to  $PF \geq 2000 \mu W m^{-1} K^{-2}$  is identified for the films prepared at  $T_R = 170$  °C. It corresponds to (i) the best in-plane chain orientation, (ii) the highest extension of planarized chain segments and (iii) the best preservation of the crystal lattice of pristine PBTTT- $^8O$  after doping with  $F_6TCNNQ$ . The contact plane of the PBTTT crystals or polymorphism determined by the rubbing temperature have apparently little influence on the final TE performances of the films. At low doping concentrations,



$F_6TCNNQ^{\bullet-}$  anions are incorporated into the lattice of PBTTT- $^8O$  with a contraction of the lattice along the  $\pi$ -stacking and expansion along the side-chain direction. However, at large dopant concentration, re-organization of the dopant radical anions in the form of dimers is observed and the lattice parameters of PBTTT- $^8O$  relaxed towards those of the pristine undoped structure. The formation of the  $(F_6TCNNQ^{\bullet-})_2$  dimers seems to be influenced by the structure of the  $C_7-O-C_4$  side chains. More generally, this study demonstrates that the identification of optimal TE performances requires a careful study of the pristine polymer film crystallization and orientation prior to doping. Precise control of structure and orientation are prerequisite to validate high performances of a given polymer semiconductor once doped. This study shows that orientation and packing of PBTTT backbones rather than chemical nature of side chains and dopants determine the physics of charge transport in doped PBTTT. Side chain layers play a key role in the hosting of dopants and can help preserve the packing of  $\pi$ -conjugated backbones. Side chain engineering of conjugated polymers impacts also the polymer film processing and may help reaching better chain alignment. Forthcoming studies will focus on the key question of long-term stability of such high performance TE polymer films.

## IV. Experimental section

### (a) Materials and thin film preparation

PBTTT- $^8O$  was synthesized following the procedure described in our previous publication ( $M_n = 30\,200$  Da and polydispersity of 1.79). The synthesis of  $F_6TCNNQ$  is given in ref. 33 and references therein. Sodium poly(styrenesulphonate) (NaPSS), anhydrous solvents (99%) used for doping (acetonitrile) and film preparation (*ortho*-dichlorobenzene) were purchased from Sigma Aldrich. PBTTT- $^8O$  films are prepared by doctor blading at  $165\text{ }^\circ\text{C}$  from a solution in ODCB ( $10\text{ g l}^{-1}$ ) on substrates of glass covered with a thin NaPSS layer (spincoated from a  $10\text{ g l}^{-1}$  aqueous solution at 3000 RPM).

### (b) Orientation and doping of thin films

The orientation of the films by high- $T$  rubbing followed the methodology described in previous publications.<sup>32,33,35</sup> For high- $T$  rubbing, a homemade set-up consisting of a rotating cylinder covered with a non-woven microfiber tissue and a translating hot plate was used. The film thickness was extracted from the UV-vis absorbance, assuming that the bulk densities of PBTTT- $C_{12}$  and PBTTT- $^8O$  are similar (which is consistent with the similar crystal lattice volumes).<sup>24,51</sup>

The doping of PBTTT- $^8O$  films with  $F_6TCNNQ$  was performed by using the incremental concentration doping (ICD) procedure<sup>33</sup> with full sample immersion for 40 s in the dopant solution of increasing concentration. No rinsing with the pure solvent was performed to avoid de-doping of the films. Both doping and rubbing were performed in a Jacomex glovebox ( $P_{N_2} \leq 1\text{ ppm}$  and  $P_{O_2} \leq 1\text{ ppm}$ ).

### (c) Structural analysis by TEM

Thin films of oriented PBTTT- $^8O$  are coated with a thin amorphous carbon film ( $<2\text{ nm}$ ) using an Edwards Auto306 evaporator. The films were removed from the glass substrate by floating on distilled water and recovered on TEM copper grids. Doping was performed inside the glovebox on the TEM grids by dipping for 40 s in the solutions of  $F_6TCNNQ$  in acetonitrile. Doped grids were rapidly transferred to the TEM for analysis. A CM12 Philips microscope (120 kV) equipped with a MVIII (Soft Imaging System) charge coupled device camera TEM was used for the structural analysis of the films (bright field and diffraction modes). The 0 0 3 reflection at  $4.5\text{ \AA}$  is not modified upon doping and was therefore used as an internal calibration to calculate the  $d_{100}$  and  $d_{020}$  reticular distances. Beam exposure was set to a minimum using the low dose system to avoid de-doping under the electron beam when the same zone is exposed for a prolonged period of time. Modeling of the structure of PBTTT- $^8O$  was performed using the appropriate modules of Cerius2 program and following the approach by Kayunkid *et al.* for P3HT and for other polymer semiconductors.<sup>52,53</sup>

### (d) Polarized UV-Vis-NIR absorption

A Varian Cary 5000 spectrometer with polarized incident light (spectral resolution of  $1\text{ nm}$ ) was used to probe the level of film orientation and the effect of film doping with  $F_6TCNNQ$  (350–2500 nm) as a function of dopant concentration. The angle of light polarization is measured with respect to the rubbing direction ( $0^\circ$  corresponding to the light polarization  $POL\parallel R$  and  $90^\circ$  corresponding to the light polarization  $POL\perp R$ ).

### (e) Charge conductivity and Seebeck coefficient

The methodology for charge transport (four-point probe) and Seebeck coefficient measurements is described in ref. 21. Devices were fabricated on glass substrates cleaned by ultrasonication in acetone, ethanol, hellmanex and deionized water ( $\times 3$  times). The cleaned substrates were dried under nitrogen and exposed to plasma prior to electrode deposition. Interdigitated gold electrodes ( $40\text{ nm}$  thick) in a four-points probe geometry (see ref. 21) were evaporated ( $0.4\text{--}0.6\text{ nm s}^{-1}$ ) through a shadow mask. The geometry of gold electrodes allows to measure both the charge transport and thermopower on a same substrate in both parallel and perpendicular directions to the rubbing. Oriented films of PBTTT- $^8O$  were floated on water and carefully recovered on the device with pre-deposited gold electrodes. They were subsequently dried under vacuum prior to doping in the glove box using the incremental concentration doping (ICD) method (see Fig. 1b).<sup>33</sup>

DC conductivity and Seebeck coefficients were measured in a Jacomex glovebox under  $N_2$  atmosphere ( $<1\text{ ppm H}_2\text{O}$  and  $<2\text{ ppm O}_2$ ). Four-point probe measurements of electrical conductivity were performed using a Keithley 2634B and a Lab Assistant Semiprobe station. The resistivity  $\rho$  was derived from the sheet resistance  $R$  following the relation  $\rho = 1.81 \cdot R \cdot t$





where  $t$  is the film thickness (the geometrical correction factor was determined following the method in ref. 21).

For the thermopower, a differential temperature method was used whereby a temperature gradient  $\Delta T$  was established across the sample along or perpendicular to the rubbing direction.  $\Delta T$  was ramped between 0 and 12 K around room temperature and the Seebeck coefficient was extracted from the slope of the thermovoltage versus  $\Delta T$ . A constantan wire was used to calibrate the Seebeck coefficient.

## Conflicts of interest

The authors declare no conflict of interest.

## Acknowledgements

Bernard Lotz is gratefully acknowledged for fruitful discussions and careful reading of the manuscript. C. Blanck and M. Schmutz are acknowledged for technical support in TEM. P. Allgayer is acknowledged for technical support with the rubbing machine and N. Zimmermann is acknowledged for technical support in pre-patterned device preparation. Financial support from ANR grant Anisotherm ANR-17-CE05-0012 (ANISOTHERM) is acknowledged. P. Durand is grateful for financial support from Région Grand'Est. This work was financially supported by the European Commission through Marie Skłodowska-Curie project HORATES (GA-955837).

## References

- 1 S. Ogawa, *Organic Electronics*, Springer, Japan, 2015, pp. 1–245.
- 2 M. Goel and M. Thelakkat, *Macromolecules*, 2020, **53**, 3632.
- 3 O. Bubnova and X. Crispin, *Energy Environ. Sci.*, 2012, **5**, 9345.
- 4 R. Kroon, D. A. Mengistie, D. Kiefer, J. Hynynen, J. D. Ryan, L. Yu and C. Müller, *Chem. Soc. Rev.*, 2016, **45**, 6147.
- 5 M. Massetti, F. Jiao, A. J. Ferguson, D. Zhao, K. Wijeratne, A. Würger, J. L. Blackburn, X. Crispin and S. Fabiano, *Chem. Rev.*, 2021, **121**, 12465.
- 6 T. Degoussée, V. Untilova, V. Vijayakumar, X. Xu, Y. Sun, M. Palma, M. Brinkmann, L. Biniek and O. Fenwick, *J. Mater. Chem. A*, 2021, **9**, 16065.
- 7 A. D. Scaccabarozzi, A. Basu, F. Aniés, J. Liu, O. Zapata-Arteaga, R. Warren, Y. Firdaus, M. I. Nugraha, Y. Lin, M. Campoy-Quiles, N. Koch, C. Müller, L. Tsetseris, M. Heeney and T. D. Anthopoulos, *Chem. Rev.*, 2021, **122**, 4420.
- 8 R. Ghosh, A. R. Chew, J. Onorato, V. Pakhnyuk, C. K. Luscombe, A. Salleo and F. C. Spano, *J. Phys. Chem. C*, 2018, **122**, 18048.
- 9 R. Ghosh, C. M. Pochas and F. C. Spano, *J. Phys. Chem. C*, 2016, **120**, 11394.
- 10 T. J. Aubry, K. J. Winchell, C. Z. Salamat, V. M. Basile, J. R. Lindemuth, J. M. Stauber, J. C. Axtell, R. M. Kubena, M. D. Phan, M. J. Bird, A. M. Spokoyny, S. H. Tolbert and B. J. Schwartz, *Adv. Funct. Mater.*, 2020, **30**, 2001800.
- 11 D. T. Scholes, S. A. Hawks, P. Y. Yee, H. Wu, J. R. Lindemuth, S. H. Tolbert and B. J. Schwartz, *J. Phys. Chem. Lett.*, 2015, **6**, 4786.
- 12 S. D. Tyler, Y. Patrick Y., R. Lindemuth Jeffrey, O. Kang Hyeyeon, G. R. Jonathan, K. Luscombe Christine, C. Spano Frank, H. Tolbert Sarah and J. Schwartz Benjamin, *Adv. Funct. Mater.*, 2017, **27**, 1702654.
- 13 I. E. Jacobs, E. W. Aasen, J. L. Oliveira, T. N. Fonseca, J. D. Roehling, J. Li, G. Zhang, M. P. Augustine, M. Mascal and A. J. Moulé, *J. Mater. Chem. C*, 2016, **4**, 3454–3466.
- 14 I. E. Jacobs and A. J. Moulé, *Adv. Mater.*, 2017, **29**, 1703063.
- 15 J. Hynynen, D. Kiefer, L. Yu, R. Kroon, R. Munir, A. Amassian, M. Kemerink and C. Müller, *Macromolecules*, 2017, **50**, 8140.
- 16 J. Hynynen, E. Järsvall, R. Kroon, Y. Zhang, S. Barlow, S. R. Marder, M. Kemerink, A. Lund and C. Müller, *ACS Macro Lett.*, 2019, **8**, 70.
- 17 R. Kroon, D. Kiefer, D. Stegerer, L. Yu, M. Sommer and C. Müller, *Adv. Mater.*, 2017, **29**, 1700930.
- 18 P. Durand, H. Zeng, T. Biskup, V. Vijayakumar, V. Untilova, C. Kiefer, B. Heinrich, L. Herrmann, M. Brinkmann and N. Leclerc, *Adv. Energy Mater.*, 2022, **12**, 2103049.
- 19 S. Ihnatsenka, *ACS Phys. Chem. Au*, 2021, **2**, 118.
- 20 V. Untilova, T. Biskup, L. Biniek, V. Vijayakumar and M. Brinkmann, *Macromolecules*, 2020, **53**, 2441.
- 21 A. Hamidi-sakr, L. Biniek, J.-L. Bantignies, D. Maurin, L. Herrmann, N. Leclerc, P. Lévêque, V. Vijayakumar, N. Zimmermann and M. Brinkmann, *Adv. Funct. Mater.*, 2017, **27**, 1700173.
- 22 V. Vijayakumar, Y. Zhong, V. Untilova, M. Bahri, L. Herrmann, L. Biniek, N. Leclerc and M. Brinkmann, *Adv. Energy Mater.*, 2019, **9**, 1900266.
- 23 V. Untilova, H. Zeng, P. Durand, L. Herrmann, N. Leclerc and M. Brinkmann, *Macromolecules*, 2021, **54**, 6073.
- 24 V. Vijayakumar, E. Zaborova, L. Biniek, H. Zeng, L. Herrmann, A. Carvalho, O. Boyron, N. Leclerc and M. Brinkmann, *ACS Appl. Mater. Interfaces*, 2019, **11**, 4942.
- 25 Y. Huang, D. H. Lukito Tjhe, I. E. Jacobs, X. Jiao, Q. He, M. Statz, X. Ren, X. Huang, I. McCulloch, M. Heeney, C. McNeill and H. Sirringhaus, *Appl. Phys. Lett.*, 2021, **119**, 111903.
- 26 Z. Liang, Y. Zhang, M. Soury, X. Luo, A. M. Boehm, R. Li, Y. Zhang, T. Wang, D.-Y. Kim, J. Mei, S. R. Marder and K. R. Graham, *J. Mater. Chem. A*, 2018, **6**, 16495.
- 27 J. Min, D. Kim, S. G. Han, C. Park, H. Lim, W. Sung and K. Cho, *Adv. Electron. Mater.*, 2022, **8**, 2101142.
- 28 A. Salleo, R. J. Kline, D. M. DeLongchamp and M. L. Chabinyc, *Adv. Mater.*, 2010, **22**, 3812.
- 29 A. Gasperini and K. Sivula, *Macromolecules*, 2013, **46**, 9349.
- 30 M. J. Lee, D. Gupta, N. Zhao, M. Heeney, I. McCulloch and H. Sirringhaus, *Adv. Funct. Mater.*, 2011, **21**, 932.
- 31 A. Hamidi-Sakr, L. Biniek, S. Fall and M. Brinkmann, *Adv. Funct. Mater.*, 2016, **26**, 408.
- 32 L. Biniek, N. Leclerc, T. Heiser, R. Bechara and M. Brinkmann, *Macromolecules*, 2013, **46**, 4014.



- 33 V. Vijayakumar, P. Durand, H. Zeng, V. Untilova, L. Herrmann, P. Algayer, N. Leclerc and M. Brinkmann, *J. Mater. Chem. C*, 2020, **8**, 16470.
- 34 Y. Karpov, T. Erdmann, M. Stamm, U. Lappan, O. Guskova, M. Malanin, I. Raguzin, T. Beryozkina, V. Bakulev, F. Günther, S. Gemming, G. Seifert, M. Hamsch, S. Mannsfeld, B. Voit and A. Kiri, *Macromolecules*, 2017, **50**, 914.
- 35 L. Biniek, S. Pouget, D. Djurado, E. Gonthier, K. Tremel, N. Kayunkid, E. Zaborova, N. Crespo-Monteiro, O. Boyron, N. Leclerc, S. Ludwigs and M. Brinkmann, *Macromolecules*, 2014, **47**, 3871.
- 36 J. Clark, J.-F. Chang, F. C. Spano, R. H. Friend and C. Silva, *Appl. Phys. Lett.*, 2009, **94**, 163306.
- 37 T. J. Prosa, M. J. Winokur and R. D. McCullough, *Macromolecules*, 1996, **29**, 3654.
- 38 D. M. DeLongchamp, R. J. Kline, Y. Jung, E. K. Lin, D. A. Fischer, D. J. Gundlach, S. K. Cotts, A. J. Moad, L. J. Richter, M. F. Toney, M. Heeney and I. McCulloch, *Macromolecules*, 2008, **41**, 5709.
- 39 R. H. Boyd and W. D. J. Phillips, *Chem. Phys.*, 1965, **43**, 2927.
- 40 A. Privitera, R. Warren, G. Londi, P. Kaienburg, J. Liu, A. Sperlich, A. E. Lauritzen, O. Thimm, A. Ardavan, D. Beljonne and M. Riede, *J. Mater. Chem. C*, 2021, **9**, 2944.
- 41 O. Zapata-Arteaga, B. Döring, A. Perevedentsev, J. Martín, J. S. Reparaz and M. Campoy-Quiles, *Macromolecules*, 2020, **53**, 609.
- 42 Y. Zhong, V. Untilova, D. Muller, S. Guchait, C. Kiefer, L. Herrmann, N. Zimmermann, M. Brosset, T. Heiser and M. Brinkmann, *Adv. Funct. Mater.*, 2022, **32**, 2202075.
- 43 D. Scheunemann, V. Vijayakumar, H. Zeng, P. Durand, N. Leclerc, M. Brinkmann and M. Kemerink, *Adv. Electron. Mater.*, 2020, **6**, 2000218.
- 44 I. E. Jacobs, G. D'Avino, V. Lemaure, Y. Lin, Y. Huang, C. Chen, T. F. Harrelson, W. Wood, L. J. Spalek, T. Mustafa, C. A. O'Keefe, X. Ren, D. Simatos, D. Tjhe, M. Statz, J. W. Strzalka, J.-K. Lee, I. McCulloch, S. Fratini, D. Beljonne and H. Sirringhaus, *J. Am. Chem. Soc.*, 2022, **144**, 3005–3019.
- 45 A. M. Glaudell, J. E. Cochran, S. N. Patel and M. L. Chabiny, *Adv. Energy Mater.*, 2015, **5**, 1401072.
- 46 H. Abdalla, G. Zuo and M. Kemerink, *Phys. Rev. B*, 2017, **96**, 241202(R).
- 47 M. Lepinoy, P. Limelette, B. Schmaltz and F. T. Van, *Sci. Rep.*, 2020, **10**, 8086.
- 48 S. D. Kang and G. J. Snyder, *Nat. Mater.*, 2016, **16**, 252.
- 49 S. A. Gregory, R. Hanus, A. Atassi, J. M. Rinehart, J. P. Wooding, A. K. Menon, M. D. Losego, G. J. Snyder and S. K. Yee, *Nat. Mater.*, 2021, **20**, 1414.
- 50 J. Liu, L. Qiu, G. Portale, M. Koopmans, G. ten Brink, J. C. Hummelen and L. J. A. Koster, *Adv. Mater.*, 2017, **29**, 1701641.
- 51 C. Y. Kao, B. Lee, L. S. Wielunski, M. Heeney, I. McCulloch, E. Garfunkel, L. C. Feldman and V. Podzorov, *Adv. Funct. Mater.*, 2009, **19**, 1906–1911.
- 52 N. Kayunkid, S. Uttiya and M. Brinkmann, *Macromolecules*, 2010, **43**, 4961.
- 53 M. Brinkmann, *Mater. Chem. Front.*, 2020, **4**, 1916.

